Available online at www.sciencedirect.com
SCIENCE DIRECT®
C. R. Mecanique 333 (2005) 235–242
COMPTES RENDUS MECANIQUE
http://france.elsevier.com/direct/CRAS2B/

Numerical simulation of expansion/compression effect on shock induced turbulent flow

Mohammad Ali Jinnah, Kazuyoshi Takayama

Shock Wave Research Center, Institute of Fluid Science, Tohoku University, 2-1-1 katahira, Aoba, Sendai 980-8577, Japan

Received 24 July 2003; accepted after revision 22 November 2004

Available online 22 January 2005

Presented by Évariste Sanchez-Palencia

Abstract

The interaction of homogeneous and isotropic turbulence with a shock wave is observed by solving the Reynolds-averaged Navier–Stokes equations with the k–ε turbulence model. All turbulent fluctuations are measured at the period of expansion in the turbulent field and during compression by the reflected shock on turbulent field, and it is observed that the longitudinal turbulent velocity fluctuation is enhanced more at the period of expansion due to incident shock wave movement far from the turbulent field. The amplification of the turbulent kinetic energy (TKE) level in the shock/turbulence interaction depends on the shock wave strength and the longitudinal velocity difference across the shock wave. On decreasing the longitudinal velocity difference across the shock, the turbulent kinetic energy (TKE) level is less amplified. The TKE level is amplified by the factor of 1.5–1.8 in the shock/turbulence interaction where the dissipation rate of TKE decreases in all cases of shock/turbulence interaction. After the shock/turbulence interaction, the turbulent dissipative-length scale is amplified slightly and the amplification of the length scales decreases when increasing the shock strength. ***To cite this article: M.A. Jinnah, K. Takayama, C. R. Mecanique 333 (2005).***

Résumé

Simulation numérique de l'effet d'expansion/compression sur un écoulement turbulent engendré par un choc. On observe l'interaction d'une turbulence homogène et isotrope avec une onde de choc en résolvant numériquement les équations de Navier–Stokes du modèle k–ε, avec le nombre de Reynolds moyennisé. Toutes les fluctuations turbulentes sont mesurées pendant la période d'expansion dans un fluide turbulent et pendant la compression par le choc réfléchi sur le champ turbulent ; on observe que les fluctuations de la vitesse de turbulence longitudinale sont rehaussées plus durant la phase d'expansion dû à l'influence de l'onde de choc incidente loin du champ turbulent. L'amplification du niveau de l'énergie cinétique turbulente (TKE) dans les interactions entre choc et turbulence dépend de l'intensité de l'onde de choc et de la différence de vitesse longitudinale le long de l'onde de choc. Si la différence de la vitesse longitudinale le long du choc diminue, l'énergie cinétique turbulence (TKE) est moins amplifiée. Le niveau de la TKE est amplifié par le facteur 1.5–1.8 dans l'interaction choc/turbulence,

E-mail address: shahjin2001@yahoo.com (M.A. Jinnah).

1631-0721/$ – see front matter
doi:10.1016/j.crme.2004.11.012

où le taux de dissipation de la TKE diminue dans tous les cas d'interaction choc/turbulence. Après cette interaction, l'échelle de longueur turbulente dissipative est légèrement amplifiée pendant que l'amplification des échelles de longueur diminue si l'intensité du choc augmente. ***Pour citer cet article : M.A. Jinnah, K. Takayama, C. R. Mecanique 333 (2005).***

Keywords: Computational fluid mechanics; Shock wave; Navier–Stokes equations; Turbulence model; Shock/turbulence interaction

Mots-clés : Mécanique des fluides numérique ; Onde de choc ; Équation de Navier–Stokes ; Modèle de turbulence ; Interaction choc/turbulence

1. Introduction

The present computations attempt to generate a compressible flow of homogeneous, isotropic turbulence in a shock tube. The shock wave and the gas flow following the shock are passed through a turbulence grid. The elementary waves formed by the diffraction of the shock at the grid propagate in a downstream direction and, after a short period, converge to form again a plane, normal shock which is weaker than the incident shock. A selected turbulent field is considered after the turbulence grid. The flow oscillations increase in the wake of turbulence grid and the flow velocity decreases due to flow interaction with the turbulence grid. After the partial reflection from the shock reflector grid, which is placed after the selected turbulent field, the reflected shock interacts with the grid-generated turbulence field. The reflected shock travels a sufficient distance before entering into the selected turbulent field, and the non-plane reflected shocks converge and become a plane shock wave after traveling sufficient distance. The aim of these computations is to compare the turbulent properties before and after the interaction of the turbulent field with different strengths of reflected shock wave. The longitudinal velocity difference across the reflected shock decreases sufficiently and the longitudinal velocity behind the reflected shock increases; these are compared to the longitudinal velocity behind the shock, reflected from the plane end wall. In these computations, all turbulent parameters are measured by decreasing the longitudinal velocity difference across the shock.

2. Numerical methods

2.1. Governing equations

The three-dimensional unsteady, compressible, Reynolds-averaged Navier–Stokes equations with the k–ε turbulence model are solved by the shock capturing method. Without external forces and heat sources, the conservative form of the non-dimensionalized governing equation in the three-dimensional Cartesian coordinate system is:

$$\frac{\partial Q}{\partial t} + \frac{\partial (F - F_v)}{\partial x} + \frac{\partial (G - G_v)}{\partial y} + \frac{\partial (H - H_v)}{\partial z} = S(Q)$$

where

$$Q = [\rho, \rho u, \rho v, \rho w, e, \rho k, \rho \varepsilon], \qquad F = [\rho u, \rho u^2, \rho uv, \rho uw, u(e+p), \rho uk, \rho u\varepsilon]$$
$$G = [\rho v, \rho uv, \rho v^2, \rho vw, v(e+p), \rho vk, \rho v\varepsilon], \qquad H = [\rho w, \rho uw, \rho vw, \rho w^2, w(e+p), \rho wk, \rho w\varepsilon]$$

and

$$F_v = [0, \tau_{xx}, \tau_{xy}, \tau_{xz}, u\tau_{xx} + v\tau_{xy} + w\tau_{xz} - q_x, k_x, \varepsilon_x]$$
$$G_v = [0, \tau_{xy}, \tau_{yy}, \tau_{yz}, u\tau_{yx} + v\tau_{yy} + w\tau_{yz} - q_y, k_y, \varepsilon_y]$$
$$H_v = [0, \tau_{xz}, \tau_{yz}, \tau_{zz}, u\tau_{xz} + v\tau_{yz} + w\tau_{zz} - q_z, k_z, \varepsilon_z]$$

Here Q is the vector of conservative variables which contains mass, momentum and energy. All variables are calculated in per unit volume. ρ is taken as the mass per unit volume. The three momentum terms in three-dimensional Cartesian coordinates system are ρu, ρv and ρw per unit volume. Total energy, e, turbulent kinetic energy, ρk and turbulent dissipative energy, $\rho\varepsilon$ are the energy terms per unit volume in these computations. F, G and H are the three inviscid flux vectors in the X-, Y- and Z-directions, respectively. Similarly, F_v, G_v and H_v are the viscous flux vectors in the three directions. Each flux vector contains mass flux, momentum flux and energy flux. ρu is the mass flux, ρu^2, ρuv, ρuw are the momentum fluxes, and $u(e+p)$, ρuk, $\rho u\varepsilon$ are the energy fluxes in the X-direction. Similarly ρv is the mass flux and ρuv, ρv^2, ρvw are the momentum fluxes and $v(e+p)$, ρvk, $\rho v\varepsilon$ are the energy fluxes in the Y-direction; ρw is the mass flux and ρwu, ρvw, ρw^2 are the momentum fluxes and $w(e+p)$, ρwk, $\rho w\varepsilon$ are the energy fluxes in the Z-direction. Also ρ is the fluid density, and u, v and w are the velocity components in each direction of the Cartesian coordinates. Since e is the total energy per unit volume, the pressure p can expressed by the following state equation for ideal gas,

$$p = (\gamma - 1)\left[e - \frac{1}{2}\rho(u^2 + v^2 + w^2)\right]$$

From the relationship between stress and strain and the assumption of Stokes, the non-dimensional stress components are as follows:

$$\tau_{xx} = \frac{\mu}{Re}\frac{2}{3}\left(2\frac{\partial u}{\partial x} - \frac{\partial v}{\partial y} - \frac{\partial w}{\partial z}\right), \quad \tau_{yy} = \frac{\mu}{Re}\frac{2}{3}\left(2\frac{\partial v}{\partial y} - \frac{\partial w}{\partial z} - \frac{\partial u}{\partial x}\right), \quad \tau_{zz} = \frac{\mu}{Re}\frac{2}{3}\left(2\frac{\partial w}{\partial z} - \frac{\partial u}{\partial x} - \frac{\partial v}{\partial y}\right)$$

$$\tau_{xy} = \frac{\mu}{Re}\left(\frac{\partial v}{\partial x} + \frac{\partial u}{\partial y}\right), \quad \tau_{yz} = \frac{\mu}{Re}\left(\frac{\partial w}{\partial y} + \frac{\partial v}{\partial z}\right), \quad \tau_{xz} = \frac{\mu}{Re}\left(\frac{\partial u}{\partial z} + \frac{\partial w}{\partial x}\right)$$

$$k_x = \frac{1}{Re}\left(\mu_l + \frac{\mu_t}{\sigma_k}\right)\frac{\partial k}{\partial x}, \quad k_y = \frac{1}{Re}\left(\mu_l + \frac{\mu_t}{\sigma_k}\right)\frac{\partial k}{\partial y}, \quad k_z = \frac{1}{Re}\left(\mu_l + \frac{\mu_t}{\sigma_k}\right)\frac{\partial k}{\partial z}$$

$$\varepsilon_x = \frac{1}{Re}\left(\mu_l + \frac{\mu_t}{\sigma_\varepsilon}\right)\frac{\partial \varepsilon}{\partial x}, \quad \varepsilon_y = \frac{1}{Re}\left(\mu_l + \frac{\mu_t}{\sigma_\varepsilon}\right)\frac{\partial \varepsilon}{\partial y}, \quad \varepsilon_z = \frac{1}{Re}\left(\mu_l + \frac{\mu_t}{\sigma_\varepsilon}\right)\frac{\partial \varepsilon}{\partial z}$$

The elements of the heat flux vector are expressed by the Fourier law of heat conduction as: $q_x = \frac{k_c}{Re}\frac{\partial T}{\partial x}$, $q_y = \frac{k_c}{Re}\frac{\partial T}{\partial y}$, $q_z = \frac{k_c}{Re}\frac{\partial T}{\partial z}$ where T is the temperature, k_c the thermal conductivity; it can be expressed as $k_c = k_l + k_t$. The expression of the thermal conductivity of the laminar part is $k_l/k_o = c_k(T/T_o)^{1.5}$ where k_o is the thermal conductivity at the ambient temperature (T_o) where the value of the coefficient c_k, depends on the temperature and the ambient gas. The expression of the thermal conductivity of the turbulent part is $k_t = c_{tk}\mu_t/Pr$ where the value of the coefficient, c_{tk} depends on the temperature and the ambient gas and Pr is the Prandtl number. The expression for laminar viscosity is $\mu_l/\mu_o = c_v(T/T_o)^{1.5}$ where μ_o is the laminar viscosity at the ambient temperature and the coefficient, c_v depends on the temperature and the ambient gas. The total viscosity $\mu = \mu_l + \mu_t$ where μ_t is the turbulent eddy viscosity, given by $\mu_t = c_\mu\rho\frac{k^2}{\varepsilon}$. The Reynolds number of the flow is defined by $Re = (\rho_c u_c l_c)/\mu_o$ where ρ_c, u_c, l_c and μ_o are, respectively, a characteristic density, a characteristic velocity, a characteristic length and the viscosity of the fluid.

The source term $S(Q)$ of the k–ε model is given by: $S(Q) = [0, 0, 0, 0, 0, P_k - \rho\varepsilon - D_k, (c_{\varepsilon 1}P_k - c_{\varepsilon 2}\rho\varepsilon)\frac{\varepsilon}{k}]$ where the production term P_k is given in Cartesian coordinates as

$$\begin{aligned} P_k = {} & \left\{2\mu_t\frac{\partial u}{\partial x} - \frac{2}{3}\left[\rho k + \mu_t\left(\frac{\partial u}{\partial x} + \frac{\partial v}{\partial y} + \frac{\partial w}{\partial z}\right)\right]\right\}\frac{\partial u}{\partial x} + \left\{2\mu_t\frac{\partial v}{\partial y} - \frac{2}{3}\left[\rho k + \mu_t\left(\frac{\partial u}{\partial x} + \frac{\partial v}{\partial y} + \frac{\partial w}{\partial z}\right)\right]\right\}\frac{\partial v}{\partial y} \\ & + \left\{2\mu_t\frac{\partial w}{\partial z} - \frac{2}{3}\left[\rho k + \mu_t\left(\frac{\partial u}{\partial x} + \frac{\partial v}{\partial y} + \frac{\partial w}{\partial z}\right)\right]\right\}\frac{\partial w}{\partial z} \\ & + \mu_t\left(\frac{\partial u}{\partial x} + \frac{\partial v}{\partial y}\right)^2 + \mu_t\left(\frac{\partial v}{\partial y} + \frac{\partial w}{\partial z}\right)^2 + \mu_t\left(\frac{\partial w}{\partial z} + \frac{\partial u}{\partial x}\right)^2 \end{aligned}$$

and the destruction term D_k, $D_k = \frac{2}{\gamma}\frac{\rho}{T}k\varepsilon$.

The mass average turbulent kinetic energy and homogeneous component of turbulent kinetic energy dissipation rate are defined by as: $k = \frac{1}{2}c_t^2(u^2 + v^2 + w^2)$ and $\varepsilon = c_m k^2 \frac{Re}{100}$.

The various constants used in the k–ε model are listed as follows: $c_\mu = 0.09$, $c_t = 0.03$, $c_m = 0.09$, $c_{\varepsilon 1} = 1.45$, $c_{\varepsilon 2} = 1.92$, $\sigma_k = 1.00$, $\sigma_\varepsilon = 1.30$.

The governing equations described above for compressible viscous flow are discretized by the finite volume method. A second-order, upwind Godounov scheme of Flux vector splitting is used to discretize the inviscid flux terms, and the MUSCL-Hancock scheme with the k–ε turbulence model is used for interpolation of the variables where the HLL-Reimann solver is used for shock capturing in the flow. Central differencing scheme is used in discretizing the viscous flux terms. The upstream of incident shock wave is set as inflow boundary condition, the properties and velocities of which are calculated from the Rankine–Hugoniot conditions with incident shock Mach number. The downstream inflow boundary condition and wall surface are used as solid boundary conditions where the gradients normal to the surface are taken as zero. All solid walls are treated as viscous solid wall boundaries. For the two-equation k–ε model on solid boundaries, μ_t is set to zero.

2.2. Grid systems and grid adaptation

Three-dimensional hexahedral cells with adaptive grid system are used for these computations. In this grid system, the cell-edge data structures are arranged in such a way that each cell contains six faces which are sequenced in one to six, and each face indicates two neighboring cells (i.e. left cell and right cell), providing all faces of a cell are vectorized by the position and coordinate in the grid system. The initial three-dimensional grid system with turbulence-generating grids are shown in Fig. 1. The physical size of each cell before adaptation is equal to $5 \times 5 \times 5$ mm.

The grid adaptation is one of the improved and computational time saving techniques, which is used in these computations. The grid adaptation is performed by two procedures: one is a refinement procedure and the other is a coarsening procedure. The refinement and coarsening operations are handled separately in the calculation. The criterion used for grid adaptation is based on the truncation error (ϵ_T) of the Taylor series expansion of the density. The truncation error indicator ϵ_T is defined for every face of a cell and given by the ratio of the second-order derivative term to the first order one of the Taylor series of density so that:

$$\epsilon_T = \max\left[\frac{|(\nabla\rho)_{lc} - (\nabla\rho)_i|}{(a_f\rho_c)/dl + |(\nabla\rho)_i|}, \frac{|(\nabla\rho)_{lc} - (\nabla\rho)_j|}{(a_f\rho_c)/dl + |(\nabla\rho)_j|}\right]$$

where c represent the location of any face of a cell and i and j represent the left cell and right cell of that face, respectively; dl is the center distance between cell i and j, $(\nabla\rho)_i$ and $(\nabla\rho)_j$ are the density gradients for cells i and j; $(\nabla\rho)_{lc} = (\rho_i - \rho_j)/dl$, where ρ_c is the density at the interface of right cell and left cell and a_f is the constant which is initially designed to prevent a zero denominator. The value of a_f used is 0.02, and it is a problem-independent parameter. The refinement and coarsening operations for any cell depend on the ϵ_T value and this ϵ_T value is determined for each face of a cell. The criterion for adaptation for any cell is:

$$\textit{Refinement} = \textit{maximum } \epsilon_T \textit{ of six faces of a cell} < \varepsilon_r$$

$$\textit{Coarsening} = \textit{maximum } \epsilon_T \textit{ of six faces of a cell} < \varepsilon_c$$

where ε_r and ε_c are the threshold values for refinement and coarsening. In these calculations, the value of ε_r used is 0.12, the value of ε_c used is 0.08, and the level of refinement is 2.

In the refinement procedure, the cells selected for refinement are divided into eight new sub cells and these are arranged in a particular sequence so that these sub cells are used correctly in the data-structure. In the coarsening procedure, the eight sub cells, which are generated from the primary cell, are restored into a primary cell. The above three-dimensional adaptation strategy is an upgraded work of two-dimensional adaptation (Sun and Takayama [7]).

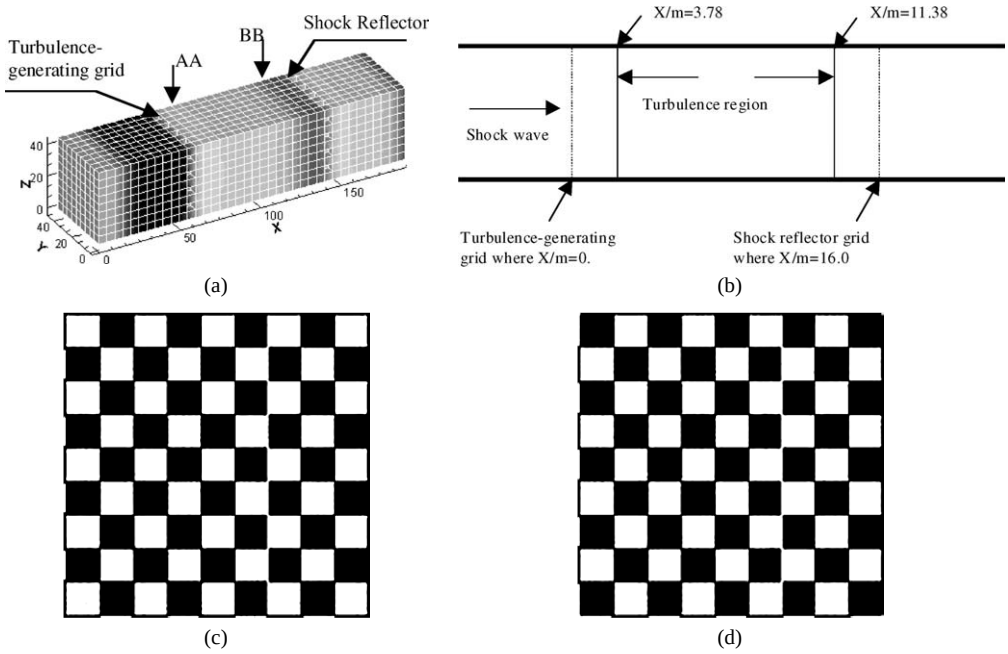

Fig. 1. (a) The position of turbulence-generating grid and shock reflector in the three-dimensional grid systems; (b) schematic diagram of the shock tube where turbulence region is shown; (c) configuration of turbulence-generating grid; (d) configuration of shock reflector grid.

Fig. 1. (a) La position de la grille engendrant la turbulence dans les systèmes de grilles tri-dimensionnel ; (b) diagramme schématique du tube de choc où l'on montre la zone de turbulence ; (c) configuration de la grille source de turbulence ; (d) configuration de la grille refléctant le choc.

3. Results and discussion

In these computations, all relevant turbulence parameters are resolved with the k–ε turbulence model and the shock wave is resolved as a solution of the Navier–Stokes equations with the techniques of shock capturing introducing. There is one disadvantage in shock reflection from plane end wall of the tube where the average longitudinal velocity behind the reflected shock is very low and the longitudinal velocity difference across the reflected shock is high. By using a proper shock reflection technique, the longitudinal velocity difference across the reflected shock is decreased.

For the numerical simulation, the computations are carried out by the shock Mach number, $M_s = 1.60$. The flow velocities behind the shock wave are determined from the Rankine–Hugoniot relations and it is seen that the flow velocity behind the shock wave of Mach number 1.60 is subsonic. To generate a compressible flow of homogeneous, isotropic turbulence; turbulence-generating grids are placed in the shock tube parallel to YZ plane, which is shown in Fig. 1 (a) and (b). The total opening area of turbulence-generating grids is 50.6% and the configuration of the turbulence-generating grids is shown in Fig. 1(c). Turbulence-generating grids are uniform in size and spacing; so the shock wave and the gas flow following the shock wave after passing through turbulence-generating grids generate a compressible flow of homogeneous, isotropic turbulence. The region between lateral plane AA and BB in Fig. 1 (a) and (b) is treated as the selected turbulent region. A grid type of shock reflector instead of an end wall is placed in the shock tube parallel to YZ plane for partial reflection of the shock and the configuration of the shock reflector is shown in Fig. 1(d). The reflected shock after reflection from the shock reflector interacts with the turbulent field in the selected turbulent region. The centerline along the longitudinal direction of turbulent region is treated as the centerline of turbulent region. 20 points of equal spacing are taken

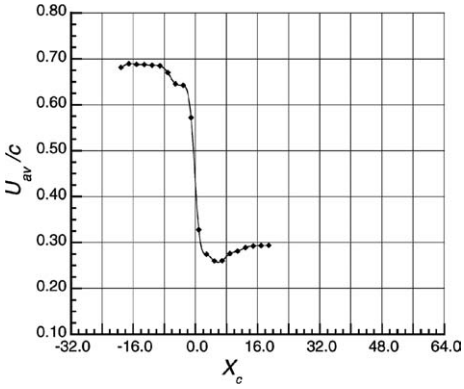

Fig. 2. Average longitudinal velocity, U_{av}/c across the shock. Here $X_c = 0.0$ mm, is the shock position where $X/m = 7.6$.

Fig. 2. La vitesse longitudinale moyenne, U_{av}/c à travers le choc. Ici $X_c = 0{,}0$ mm est la position du choc où $X/m = 7{,}6$.

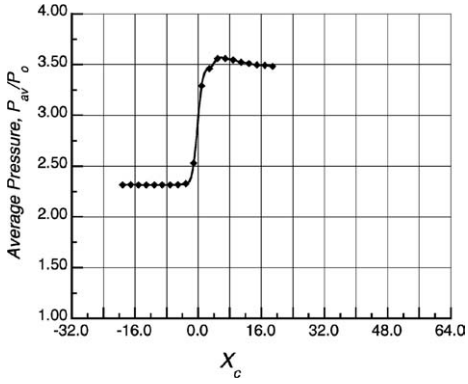

Fig. 3. Average pressure, P_{av}/P_o across the shock. Here $X_c = 0.0$ mm, is the shock position where $X/m = 7.6$ and P_o is the STD atmospheric pressure.

Fig. 3. Pression moyenne P_{av}/P_o à travers la zone du choc (ici $X_c = 0{,}0$ mm est la position du choc où $X/m = 7{,}6$, et P_o est la pression atmosphérique standard).

on the centerline of turbulent region and all turbulent parameters (velocity fluctuations, pressure fluctuations etc.) are computed on these 20 points. The lateral planes intersect these points and parallel to the YZ plane are treated as grid-data plane and the grids inside the turbulent region cut by the grid-data plane are the grids on the grid-data plane. The value of the turbulent parameter on the centerline of the turbulent region is the average value of all the grid value of that parameter on the grid-data plane and in these computations, the grids adjacent to the boundary are not taken into account due to viscous effect. The longitudinal distance (X/m) of any point on the centerline of turbulent region is determined from the turbulence-generating gird where m is the maximum dimensional length of a grid in the grid systems.

The RMS longitudinal velocity fluctuations, $\langle u\rangle/U$ are determined along the longitudinal distance (X/m) where U is the flow velocity behind the incident shock wave and it is determined for $M_s = 1.60$ by the Rankine–Hugoniot relations. The RMS longitudinal velocity fluctuations, $\langle u\rangle$ are the average fluctuation on the points of the centerline of the turbulent region. The RMS longitudinal velocity fluctuation is given by: $\langle u\rangle = \sqrt{(\sum_{i=1}^{n}(u_i - U_{\text{av}})^2)/n}$ where u_i is the instantaneous longitudinal velocity, the average velocity, U_{av} in X-direction $= (\sum_{i=1}^{n} u_i)/n$ and n is the number of grids on the grid-data plane where the grids near the boundary are not taken into account due to viscous effects. The dimensionless longitudinal velocity, U_{av}/c across the reflected shock is determined where c is the local sound velocity. The longitudinal velocity, U_{av}/c across the shock, is a characteristic shape, shown in Fig. 2 and it is seen that the longitudinal velocity behind the reflected shock increases substantially as compare to the shock reflection from the plane end wall. Similarly the average pressure, P_{av}/P_o is determined along the centerline of the turbulent region, which is shown in Fig. 3, and it is seen that the pressure profile obeys the shock reflection theory. The RMS longitudinal velocity fluctuations, $\langle u\rangle/U$ are determined along the centerline of turbulent region at the period of expansion and compression. The characteristics curves, (a) and (b) in Fig. 4 show the turbulence intensity magnitude at the period of expansion when the position of the shock is near and far, respectively, from the turbulent region. Similarly the characteristics curves, (a) and (b) in Fig. 5 show the longitudinal turbulence intensity magnitude during the compression on the turbulent field, when the position of shock far from and near the turbulent region. The characteristics curve, (c) in Fig. 5 shows the longitudinal turbulence intensity along the centerline of turbulent region after the reflected shock/homogeneous turbulence interaction. After the shock/turbulence interaction, the longitudinal turbulence intensity is amplified by the factor of 1.2–1.4 and the turbulent kinetic energy (TKE) level is amplified by the factor of 1.5–1.8; the above amplification

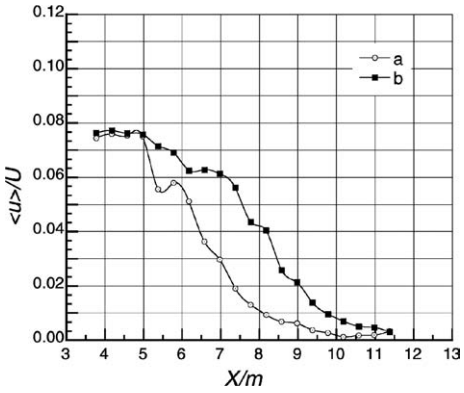

Fig. 4. Longitudinal velocity fluctuations, $\langle u\rangle/U$ along the centerline of turbulent region at the period of expansion for the positions of shock: (a) near turbulent region i.e. $X_s/m = 12.5$ and before reflection; (b) far from turbulent region i.e. $X_s/m = 15.5$ and before reflection. Here X_s is the shock wave position from turbulence-generating grid.

Fig. 4. Fluctuations de vitesse longitudinale $\langle u\rangle/U$ le long de la ligne médiane de la zone de turbulence pendant la période d'expansion, correspondant qux positions du choc : (a) près de la zone de turbulence, c'est-à-dire pour $X_s/m = 12{,}5$ et avant la réflexion ; (b) loin de la zone de turbulence, c'est-à-dire pour $X_s/m = 15{,}5$ et avant la réflexion. Ici X_s est la position de l'onde de choc comptée à partir de la grille source de turbulence.

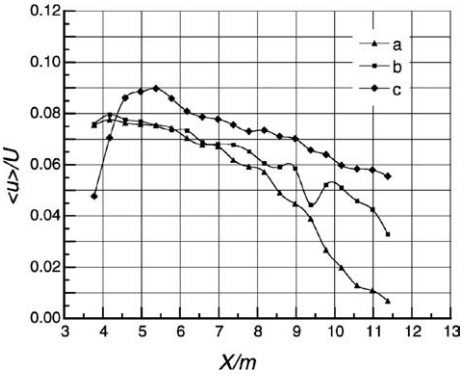

Fig. 5. Longitudinal velocity fluctuations, $\langle u\rangle/U$ along the centerline of turbulent region during compression on turbulent field for the positions of shock: (a) far from turbulent region i.e. $X_s/m = 15.0$ and after reflection; (b) near turbulent region i.e. $X_s/m = 13.0$ and after reflection; (c) after the interaction with turbulent field i.e. $X_s/m = 2.0$.

Fig. 5. Fluctuations de vitesse longitudinale, $\langle u\rangle/U$ le long de la ligne médiane de la zone de turbulence, pendant la compression correspondant aux positions du choc : (a) loin de la zone de turbulence, soit pour $X_s/m = 15{,}0$ et après réflexion ; (b) près de la zone de turbulence, soit pour $X_s/m = 13{,}0$ et après réflexion ; (c) après l'interaction avec le champ turbulent, soit pour $X_s/m = 2{,}0$.

Table 1
Comparison with other results

Amplification factor for:	Partial reflection ($M_s = 1.60$)	Full reflection ($M_s = 1.50$)	Full reflection ($M_s = 2.00$)	Full reflection ($M_s = 2.20$)	Honkan and Andreopoulos ($M_s = 1.354$)	Briassulis	Lee et al. ($M_s = 1.02$–1.20)	Rotman ($M_s = 1.01$–1.50)
Turbulence intensity	1.2–1.4	1.98–2.12	1.35–1.44	1.16–1.22	1.1–1.48	$\leqslant 2$	$\leqslant 2$	
TKE level	1.5–1.8	3.09–3.41	2.00–2.14	1.65–1.75				$\leqslant 2$

factors are higher in the case of plane end wall reflection, which were computed by Jinnah and Takayama [1]. The two-dimensional computational results inside the Mach number range 1.01–1.50, conducted by Rotman [2], the maximum amplification factor of TKE level was 2.00. A comparison, Table 1, is provided below to compare the present results of the amplification of the turbulence intensity and TKE level with the results of reference [1] and other references.

The turbulent dissipation rates are determined before and after the interaction of the shock wave with the turbulent field. It is observed that in all cases the dissipation rate decreases after the interaction of shock wave with turbulent field and the dissipation rate of turbulent kinetic energy level are higher values in interaction of shock wave with strong turbulent field.

The dissipative-length scale is defined by the expression of $k^{3/2}/\varepsilon$ with the turbulent kinetic energy, $k = (\sum_{i=1}^{n} k_i)/n$; k_i is the instantaneous turbulent kinetic energy for any grid on the grid-data plane and n is the number of grids on the grid-data plane where the grids adjacent to the boundary are not taken into account due to viscous effect. Similarly the dissipation rate is $\varepsilon = (\sum_{i=1}^{n} \varepsilon_i)/n$ where ε_i is the instantaneous turbulent kinetic energy dissipation rate for any grid on the grid-data plane. The amplification of dissipative-length scale is the ratio

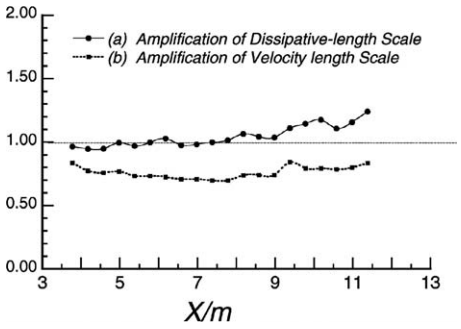

Fig. 6. (a) The amplification of dissipative-length scale along the centerline of the turbulent region; (b) the amplification of velocity length scale along the centerline of the turbulent region.

Fig. 6. (a) L'amplification de l'échelle de longueur dissipative le long de la ligne médiane de zone de turbulence ; (b) l'amplification de l'échelle de vitesse le long de la ligne médiane de zone de turbulence.

of the dissipative-length scale after interaction to the dissipative-length scale before interaction. The amplifications of dissipative-length scale are determined along the certerline of the turbulent region, which is shown in Fig. 6(a). It is observed that the amplifications of dissipative-length scale increase slightly in interaction of shock wave with turbulent field. Due to stronger compressibility effects, the amplifications of dissipative-length scale in strong shock/turbulence interaction decrease. The DNS data of Lee et al. [3] and Hannappel and Friedrich [4] indicate that velocity length scale and dissipative-length scale decrease through the shock interaction. The dissipative-length scale in the experiment of Honkan and Andreopoulos [5] was found to increase after the interaction. DNS results of Lee et al. [6] have indicated a small increase of dissipative-length scales through weak shock interactions.

The velocity length scale is defined by the expression of $k^{1/2}$. The amplification of velocity length scale is the ratio of the velocity length scale after interaction to the velocity length scale before interaction. The amplifications of velocity length scale are determined along the certerline of the turbulent region, which is shown in Fig. 6(b). It is observed that the amplifications of velocity length scale decrease in interaction of shock wave with turbulent field and due to stronger compressibility effects; the amplifications of velocity length scale in strong shock/turbulence interaction decrease more.

4. Conclusions

The present computations indicate that the turbulent kinetic energy levels are amplified less due to decreasing the longitudinal velocity difference across the shock. After interaction, the dissipation rate of turbulent kinetic energy decreases in all the cases of shock/turbulence interaction. The outcomes of shock/turbulence interaction depend on the compressibility effect on turbulent field.

References

[1] M.A. Jinnah, K. Takayama, Numerical simulation of shock Mach effect on normal shock/homogeneous turbulence interaction, in: Computational Methods and Experimental Measurements XI, Proc. of the Eleventh International CMEM-2003 Conference, 2003, pp. 505–515.
[2] D. Rotman, Shock wave effects on a turbulent flows, Phys. Fluids A 3 (7) (1991) 1792–1806.
[3] S. Lee, S.K. Lele, P. Moin, Direct numerical simulation of isotropic turbulence interacting with a weak shock wave, J. Fluid Mech. 251 (1993) 533–562.
[4] R. Hannappel, R. Friedrich, Direct numerical simulation of a Mach 2 shock interacting with isotropic turbulence, Appl. Sci. Res. 54 (1995) 205–221.
[5] A. Honkan, J. Andreopoulos, Rapid compression of grid-generated turbulence by a moving shock wave, Phys. Fluids A 4 (1992) 2562–2572.
[6] S. Lee, S.K. Lele, P. Moin, Interaction of isotropic turbulence with a strong shock wave, AIAA paper 94-0311 Dept. Mech. Eng., Stanford University, CA, 1994.
[7] M. Sun, K. Takayama, Conservative smoothing on an adaptive quadrilateral grid, J. Comput. Phys. 150 (1999) 143–180.